Journal of Materials Chemistry

Cite this: J. Mater. Chem., 2012, 22, 7697

www.rsc.org/materials

COMMUNICATION

Tightly connected MnO_2–graphene with tunable energy density and power density for supercapacitor applications†

Chih-Yao Chen,[a] Chen-Yen Fan,[a] Ming-Tsung Lee[a] and Jeng-Kuei Chang*[abc]

Received 20th December 2011, Accepted 5th March 2012
DOI: 10.1039/c2jm16707g

MnO_2 nanoparticles uniformly distributed and tightly anchored on graphene are prepared using an ethanol-assisted graphene-sacrifice reduction method, producing composite electrodes with tunable energy density (up to 12.6 Wh kg^{-1}) and power density (up to 171 kW kg^{-1}) *via* rational design of the oxide/graphene ratio.

The depletion of fossil fuels coupled with increasing demand for energy and growing concerns about pollution and global warming have led to accelerated development of clean energy conversion/storage systems that can meet future power requirements. Supercapacitors, including electric double-layer capacitors (EDLCs) and pseudocapacitors, are considered promising candidates for effective energy storage due to their high power density, long cycle life, and low maintenance cost.[1,2] They have been applied in hybrid electric vehicles, consumer electronics, medical devices, and military missile systems.[3] Pseudocapacitors, whose capacitance is mainly attributed to the continuous and reversible redox reaction of electrode materials, have higher energy density (at the expense of power capability and cyclic stability) than that of EDLCs and thus have become increasingly attractive.[4] Improving the power and cycle life performance of pseudocapacitors and extending their charge storage capacity to approach that of batteries are important research goals.

MnO_2 is known as a potential pseudocapacitive material with satisfactory specific capacitance, high abundance, low cost, and environmental benignity.[5] However, due to its extremely low electrical conductivity (~10^{-5} to 10^{-6} S cm^{-1}) and typical densely packed structure, the rate capability and reversibility of MnO_2 electrodes are limited.[6] It is highly desirable to increase the reactivity and utilization of MnO_2 by electrically wiring up the oxide particles with conducting mats and by creating porosity for ionic (electrolyte) transport within the electrode.

Graphene, a two-dimensional sheet of sp^2-hybrized carbon atoms packaged into a honeycomb lattice structure, is characterized by high conductivity, large surface area, great chemical stability, high mechanical flexibility, and light weight. Accordingly, graphene outperforms other carbon nanostructures in a variety of energy-related applications.[7] Recently, graphene has been applied as an EDLC material in consideration of its extremely high surface area.[8] However, graphene EDLCs may not meet the expected electrochemical performance because of the serious agglomeration and restacking of neighboring graphene sheets due to van der Waals interactions.[9] Graphene may be more suitable for pseudocapacitors, especially for incorporation in MnO_2 electrodes. The introduction of graphene sheets can significantly improve the electronic conductivity of the composite electrode. Moreover, graphene's high surface area helps disperse oxide particles and form electrolyte-accessible channels within the electrode. The oxide particles between graphene sheets can suppress restacking, optimizing both the double-layer capacitance and pseudocapacitance in the composite electrode.

A few studies have recently attempted to synthesize MnO_2/graphene nanocomposites using different approaches.[10–13] The specific capacitance of the composite electrode prepared by electrodeposition is as high as 328 F g^{-1}.[11] It is believed that the connectivity between the two hetero-substances is a critical factor governing the ultimate capacitive performance.[14] An intimate contact of oxide/graphene is desired since it facilitates electronic conduction, which benefits reaction kinetics and oxide utilization. Moreover, good adhesion prevents detachment and aggregation during charging/discharging, improving the electrode cyclic stability. The present study proposes a facile, low-cost, and scalable method for tightly anchoring MnO_2 onto graphene. The energy density and power density of the electrode can be tailored by adjusting the ratio of oxide to graphene in accordance with the application requirements.

Graphene nanosheets were prepared using a modified Staudenmaier method;[15] the details are provided in the ESI†. Briefly, natural graphite powder (Alfa Aesar; with a particle size of ~70 μm and a purity of 99.999%) was chemically oxidized (using H_2SO_4, HNO_3, and $KClO_3$) to produce graphite oxide (GO). The common Hummers oxidation method would introduce residual Mn^{7+}, which may interfere with our experiment and thus it is not adopted. The difference between the Staudenmaier and Hummers processes is compared in the literature.[16] Exfoliation of GO was then carried out by rapidly heating it to 1050 °C in an inert Ar atmosphere. After the thermal reduction at high temperature, GO was reduced to graphene, which has a higher electrical conductivity and is thus more suitable for use in supercapacitors.[17] The prepared graphene nanosheets

[a]*Institute of Materials Science and Engineering, National Central University, Taoyuan, Taiwan. E-mail: jkchang@ncu.edu.tw; Fax: +886-3-2805034*
[b]*Department of Chemical and Materials Engineering, National Central University, Taoyuan, Taiwan*
[c]*Department of Mechanical Engineering, National Central University, Taoyuan, Taiwan*
† Electronic supplementary information (ESI) available. See DOI: 10.1039/c2jm16707g

showed a distinct Raman 2D band (see ESI, Fig. SI1†) and a uniform thickness of approximately 4 nm (Fig. SI2†); both analyses indicate that our product is few-layer graphene. Graphene in a highly reduced state can reduce Mn^{7+} *via* the self-sacrifice reaction:[18]

$$C \rightarrow C^{+} + e^{-} \quad (1)$$

This led to the direct growth of MnO_2 on its surface. The redox exchange between C and Mn^{7+} made the deposited MnO_2 closely attached to the graphene nanosheets.

It was found that with only the graphene-sacrifice reduction process, the amount of deposited MnO_2 (from $KMnO_4$ solution) was limited (less than 3% in the composite) since the initially formed oxide hindered further redox reaction. Ethanol, a mild reductant,[19] was used as an assisted reducing agent in this work; the pH was adjusted to ~14 (by KOH) to further decelerate the reduction reaction (detailed procedures are in the ESI†). If the activity of the additional reductant was too strong, the deposition reaction of the oxide would become excessively violent, leading to the sacrifice reduction reaction becoming minor. As a result, only a physical mixing of MnO_2 and graphene would be obtained (loose contact could be expected). Using the proposed ethanol-assisted graphene-sacrifice concept, composites were synthesized with MnO_2 to graphene weight ratios of 99/1, 97/3, and 90/10 (evaluated using TGA); the samples are referred to as MnO_2/GNS-99/1, MnO_2/GNS-97/3, and MnO_2/GNS-90/10, respectively.

Microstructures of the samples were examined using scanning electron microscopy (SEM). Fig. 1(a) shows a SEM micrograph of a plain MnO_2 sample (without graphene). The particle size is in the range of 100–300 nm with some agglomeration. X-ray and electron diffraction (Fig. SI3 and SI4†) results confirm that the sample was nanocrystalline α-MnO_2 (JCPDS card no. 44-0141). The typical morphology of the prepared graphene is shown in Fig. 1(b); carbon sheets with some wrinkles can be observed. Fig. 1(c)–(e) show SEM micrographs of MnO_2/GNS-99/1, MnO_2/GNS-97/3, and MnO_2/GNS-90/10, respectively. It was found that the MnO_2 was highly dispersed on graphene. Since the high-surface-area graphene acted as a template to host the oxide, the agglomeration was lower than that for the plain MnO_2 sample. With increasing graphene content, the porosity of the composites increased; the BET surface area increased from 120 $m^2\ g^{-1}$ to 250 $m^2\ g^{-1}$ when 10 wt% graphene was incorporated into the oxide. It was also noted that the particle size of the reduced oxide was smaller and more uniform (80–100 nm) when incorporated with graphene. The released electrons from eqn (1) can cause a heterogeneous reduction of MnO_2 on graphene. Since there are plenty of favorable nucleation sites for oxide deposition on graphene, tiny oxide crystals with a centralized size distribution were obtained. A TEM micrograph that reveals uniformly distributed and well-adhered oxide particles on graphene is shown in the ESI (Fig. SI5†).

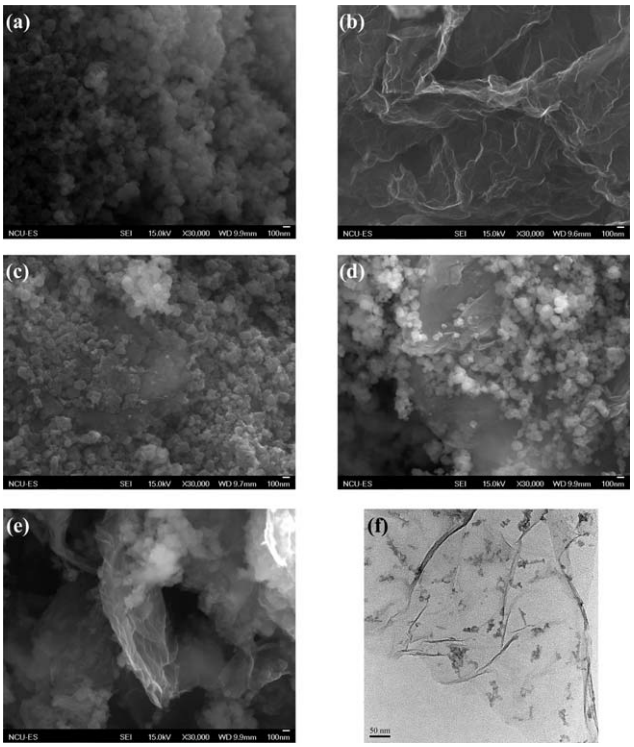

Fig. 1 SEM micrographs of the (a) plain MnO_2, (b) pristine graphene, (c) MnO_2/GNS-99/1, (d) MnO_2/GNS-97/3, and (e) MnO_2/GNS-90/10 samples. (f) TEM image of the MnO_2/GNS-90/10 sample after detaching the oxide particles.

The redox interaction of C and Mn^{7+} also implies an intimate contact between graphene/MnO_2. The good adhesion can be depicted in the transmission electron microscopy (TEM) image in Fig. 1(f). Before this TEM observation, prolonged high-power ultrasonication was used to force detachment (or dissolution) of the deposited MnO_2 particles. As shown, the graphene nanosheet was decorated with the oxide footprints. This indicates that a strong chemical interaction (instead of just infirm attachment) may exist. The oxide stains are clear evidence of the tight connection between graphene and MnO_2. The selection of an appropriate reducing agent (such as ethanol) is crucial for the proposed synthesis route. A strong reductant would cause rapid oxide deposition in the solution (rather than on graphene), leading to only a physical blend of the two constituents.

Fig. 2(a) shows the cyclic voltammetry (CV) data of the three MnO_2–graphene composite electrodes, a plain MnO_2 electrode, and a plain graphene electrode measured in 3 M KCl aqueous solution with a potential sweep rate of 5 mV s^{-1} (the electrode preparation process is described in the ESI†). The rectangular and mirror-image characteristics of the curves indicate ideal capacitive behavior. Their specific capacitance (C, based on the mass of the composite) can be quantitatively evaluated using:

$$C = Q_m/\Delta V \quad (2)$$

where Q_m is the specific voltammetric charge integrated from both the anodic and cathodic CV scans, and ΔV is the potential range. The capacitance of the plain MnO_2 electrode is 215 F g^{-1}, which is close to the value reported in the literature.[20,21] With even a small amount of incorporated graphene, the specific capacitance increases to 365 F g^{-1} (MnO_2/GNS-99/1). This indicates a great benefit of incorporating graphene in the energy-storage electrode; a synergistic capacitance can be obtained because the electrode microstructure has been optimized. Further increasing the graphene content caused the capacitance to decrease; the MnO_2/GNS-97/3 and MnO_2/GNS-90/10 electrodes show values of 310 and 265 F g^{-1}, respectively. Since graphene has an inferior capacitance (as shown in the figure), excessive addition is unfavorable. The specific capacitance of 365 F g^{-1} is among the highest values reported in the literature[11,13] for

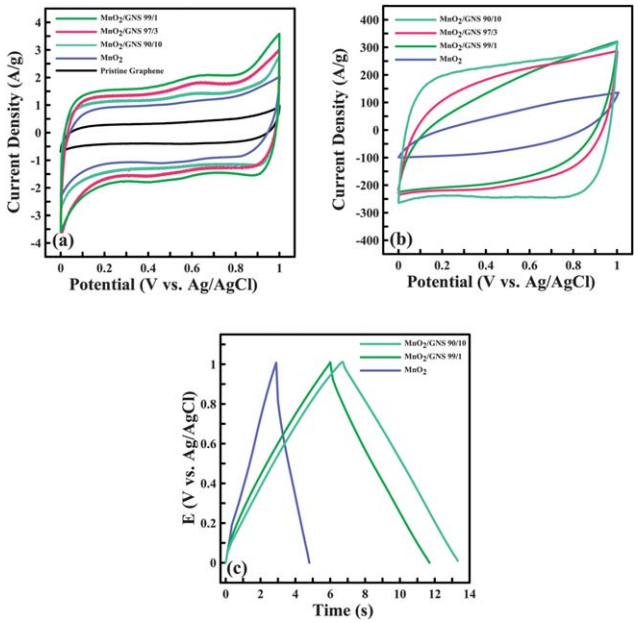

Fig. 2 Cyclic voltammograms of various electrodes measured in 3 M KCl aqueous solution with potential sweep rates of (a) 5 mV s^{-1} and (b) 1000 mV s^{-1}. (c) Chronopotentiograms of various electrodes measured at an applied current density of 50 A g^{-1}.

MnO_2–graphene nanocomposites. The high specific capacitance can be attributed to the intimate contact between the oxide and graphene, which connects the low-conductivity MnO_2 particles, thus enhancing the utilization of the electrode in the pseudocapacitive reaction. Moreover, the smaller size and lower agglomeration of MnO_2 on graphene ensure a large interface area for the electrolyte, improving the electrode reactivity.

High-rate capability is another key performance index for supercapacitor electrodes. Fig. 2(b) shows voltammograms recorded at a high scan rate of 1000 mV s^{-1}. That for the plain MnO_2 electrode shows a spindle shape with a small response current, reflecting a large internal resistance and an inferior capacitive performance. The calculated capacitance was 68 F g^{-1}, which is ~32% of that measured at 5 mV s^{-1}. With increasing graphene content in the composites, the CV enclosed area became larger and gradually approached a rectangular shape. The MnO_2/GNS-99/1, MnO_2/GNS-97/3, and MnO_2/GNS-90/10 electrodes showed capacitances of 167 F g^{-1} (46% of that at 5 mV s^{-1}), 183 F g^{-1} (59%), and 227 F g^{-1} (86%), respectively. The capacitance-retained ratio of 86% after a potential sweep rate increase of a factor of forty is the highest for MnO_2–graphene composites reported in the literature.[10–13] Importantly, the low amount of graphene used in the proposed electrode (<10%) can considerably decrease cost. The superior high-rate performance is ascribed to the following factors. First, the highly conductive graphene nanosheets in the composite electrode can form a three-dimensional conducting network for fast electron transfer between the oxide and current collector. Second, the high dispersion of the nano-sized oxide particles on graphene can shorten the ion diffusion path. Third, the MnO_2 particles attached on the graphene serve as spacers to support the adjacent nanosheets, creating high porosity in the nanocomposites (as shown in Fig. 1) for electrolyte accessibility. Accordingly, the electronic and ionic conductivities are optimized, resulting in the excellent high-rate capability.

Chronopotentiometry analytic results of various electrodes are shown in Fig. 2(c). The triangular appearance of the curves confirms the capacitive behavior of the electrodes. As shown, the plain MnO_2 has the shortest charge/discharge period, indicating the lowest capacitance, which is consistent with the CV data. A clear iR drop, attributed to a significant internal resistance, was found at the initial charge or discharge stage. However, the MnO_2–graphene composites (especially for MnO_2/GNS-90/10) exhibited an ideal supercapacitor performance even at the extremely high applied current density of 50 A g^{-1}. The symmetric and near-linear characteristics (with little iR drop) of the anodic and cathodic branches suggest that the composite electrode prepared using the proposed synthesis protocol has excellent redox activity and kinetics. According to Fig. 2(c), the current efficiency of the plain MnO_2 electrode is only ~70%, whereas those of the graphene-incorporated electrodes are almost 100%. The high efficiency translates to great reversibility, less heat dissipation, and superior cyclic stability during the charge/discharge operation. A symmetric two-electrode configuration, which mimics the practical packaged cell, was also used to evaluate the supercapacitor performance.[22] The galvanic charge–discharge curves measured at various current densities are shown in Fig. SI6†. We found that the measured capacitances are approximately half of those evaluated from the three-electrode configuration, simply because the two-electrode cell consists of two series-connected capacitive electrodes.

Fig. 3 shows the Ragone plot of the prepared electrodes. The energy density and power density (based on active materials on both the electrodes) are derived from the two-electrode charge–discharge curves measured at various rates. The MnO_2–graphene composites outperform the plain oxide electrode in terms of both properties. The maximum energy densities of the MnO_2/GNS-99/1, MnO_2/GNS-97/3, and MnO_2/GNS-90/10 electrodes are 50.2, 42.9, and 36.6 Wh kg^{-1}, respectively. However, the MnO_2/GNS-90/10 electrode exhibited the best powder density (400 kW kg^{-1} with a reasonable energy density of 20 Wh kg^{-1}). This performance is better than those of recently reported MnO_2–graphene,[11–13] $Ni(OH)_2$–graphene,[23] and RuO_2–graphene[24] composite electrodes. Moreover, it should be emphasized that this is the first work demonstrating that the energy and power performance of a supercapacitor electrode can be tuned by adjusting the ratio of the oxide to graphene.

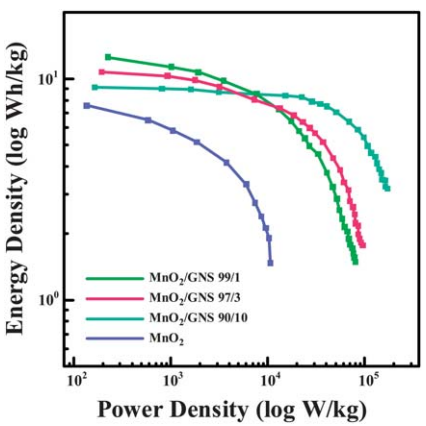

Fig. 3 Ragone plots of the synthesized MnO_2/GNS-99/1, MnO_2/GNS-97/3, MnO_2/GNS-90/10 composite electrodes. The performance of a plain MnO_2 electrode is also shown for comparison.

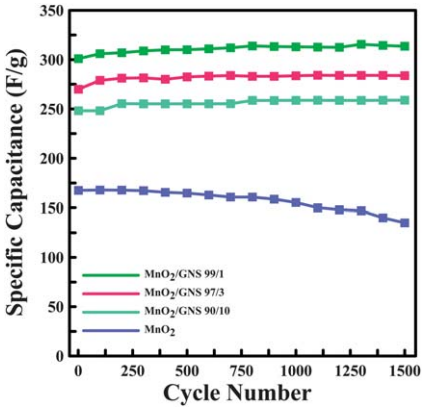

Fig. 4 Variations of the specific capacitance, measured at a CV sweep rate of 50 mV s^{-1}, *versus* the charge/discharge cycle number for the various electrodes prepared.

The electrochemical stability of the electrodes was also evaluated using CV; the obtained data are shown in Fig. 4. The plain MnO_2 shows a clear deterioration (~20% decay) after 1500 cycles, whereas the three composite electrodes show excellent cyclic stability. The slight increase of capacitance may be associated with the adjustment of the graphene–MnO_2 inter-configuration during cycling, leading to a more favorable redox posture of the composite electrodes. Interestingly, only 1 wt% graphene is sufficient to significantly improve the electrode cycle life. The favorable electronic and ionic transport within the composite electrode benefits the reaction homogeneity and reversibility. The tight adhesion between MnO_2 and graphene suppresses the detachment and re-agglomeration of the oxide nanoparticles. Moreover, graphene acts as a flexible cushion that can accommodate the volume change and the associated release of strain generated during charge/discharge cycling. As a result, the great durability of the electrode can be obtained.

In conclusion, a facile, low-cost, and scalable approach for uniformly distributing and tightly anchoring nano-sized MnO_2 onto graphene was originally developed. Due to the unique particle-sheet structure, only 1 wt% graphene incorporation can significantly increase the specific capacitance (from 215 to 365 F g^{-1}) and cyclic stability of the supercapacitor electrode. The energy density and power density of the composite electrode can be tailored by adjusting the oxide to graphene ratio. The present results contribute an important advance in the field of supercapacitors; the proposed electrode has great potential for a wide variety of applications, such as electric vehicles and heavy machinery. Besides, the proposed synthesis protocol and composite design concept can also be applicable to other energy storage/conversion systems to improve the electrode performance and to better fit the required properties as well.

The financial support of this work by the National Science Council of the Republic of China under grant NSC 99-2218-E-008-007-MY3 is gratefully appreciated.

References

1 B. E. Conway, *Electrochemical Supercapacitors, Scientific Fundamentals and Technological Applications*, Kluwer Academic/Plenum Press, New York, 1999.
2 P. Simon and Y. Gogotsi, *Nat. Mater.*, 2008, **7**, 845.
3 P. J. Hall, M. Mirzaeian, S. I. Fletcher, F. B. Sillars, A. J. R. Rennie, G. O. Shitta-Bey, G. Wilson, A. Cruden and R. Carterf, *Energy Environ. Sci.*, 2010, **3**, 1238.
4 X. Zhao, B. M. Sanchez, P. J. Dobson and P. S. Grant, *Nanoscale*, 2011, **3**, 839.
5 W. F. Wei, X. W. Cui, W. X. Chen and D. G. Ivey, *Chem. Soc. Rev.*, 2011, **40**, 1697.
6 A. E. Fischer, K. A. Pettigrew, D. R. Rolison, R. M. Stroud and J. W. Long, *Nano Lett.*, 2007, **7**, 281.
7 D. A. C. Brownson, D. K. Kampouris and C. E. Banks, *J. Power Sources*, 2011, **196**, 4873.
8 M. D. Stoller, S. J. Park, Y. W. Zhu, J. H. An and R. S. Rouff, *Nano Lett.*, 2008, **8**, 3498.
9 Y. Wang, Z. Q. Shi, Y. Huang, Y. F. Ma, C. Y. Wang, M. M. Chen and Y. S. Chen, *J. Phys. Chem. C*, 2009, **113**, 13103.
10 S. Chen, J. W. Zhu, X. D. Wu, Q. F. Han and X. Wang, *ACS Nano*, 2010, **4**, 2822.
11 Q. Cheng, J. Tang, J. Ma, H. Zhang, N. Shinya and L. C. Qin, *Carbon*, 2011, **49**, 2917.
12 Z. Fan, J. Yan, T. Wei, L. Zhi, G. Ning, T. Li and F. Wei, *Adv. Funct. Mater.*, 2011, **21**, 2366.
13 G. H. Yu, L. B. Hu, M. Vosgueritchian, H. L. Wang, X. Xie, J. R. McDonough, X. Cui, Y. Cui and Z. N. Bao, *Nano Lett.*, 2011, **11**, 2905.
14 S. B. Ma, K. Y. Ahn, E. S. Lee, K. H. Oh and K. B. Kim, *Carbon*, 2007, **45**, 375.
15 L. Staudenmaier, *Ber. Dtsch. Chem. Ges.*, 1898, **31**, 1481.
16 O. C. Comption and S. T. Nguyen, *Small*, 2010, **6**, 711.
17 W. Gao, L. B. Alemany, L. Ci and P. M. Ajayan, *Nat. Chem.*, 2009, **1**, 403.
18 S. B. Ma, Y. H. Lee, K. Y. Ahn, C. M. Kim, K. H. Oh and K. B. Kim, *J. Electrochem. Soc.*, 2006, **153**, C27.
19 Y. Ma, J. Luo and S. L. Suib, *Chem. Mater.*, 1999, **11**, 1972.
20 J. K. Chang and W. T. Tsai, *J. Electrochem. Soc.*, 2003, **150**, A1333.
21 P. Raguphaty, D. H. Park, G. Campet, H. N. Vasan, S. J. Hwang, J. H. Choy and N. Munichandraiah, *J. Phys. Chem. C*, 2009, **113**, 6303.
22 M. D. Stoller and R. S. Ruoff, *Energy Environ. Sci.*, 2010, **3**, 1294.
23 H. L. Wang, H. S. Casalongue, Y. Y. Liang and H. J. Dai, *J. Am. Chem. Soc.*, 2010, **132**, 7472.
24 Z. S. Wu, D. W. Wang, W. Ren, J. Zhao, G. Zhou, F. Li and H. M. Cheng, *Adv. Funct. Mater.*, 2010, **20**, 3595.

